Regular Article

PHYSICAL CHEMISTRY RESEARCH
Published by the
Iranian Chemical Society
www.physchemres.org
info@physchemres.org

***Phys. Chem. Res.**, Vol. 2, No. 1, 76-89, June 2014.*
DOI: 10.22036/pcr.2014.4012

Ultrasonic-assisted Method for Preparation of Cu-doped ZnS Nanoparticles in Water as a Highly Efficient Visible Light Photocatalyst

Z. Poormohammadi-Ahandani, A. Habibi-Yangjeh* and M. Pirhashemi
Department of Chemistry, Faculty of Sciences, University of Mohaghegh Ardabili, P.O. Box 179, Ardabil, Iran
(Received 22 June 2013, Accepted 22 December 2013)

Ultrasonic-assisted method was applied for preparation of Cu^{2+}-doped ZnS nanoparticles (mole fractions of Cu^{2+} ions are 0.000, 0.015, 0.030 and 0.060) in water as a template-free and green method at 30 min. The prepared nanoparticles were investigated by powder X-ray diffraction (XRD), scanning electron microscopy (SEM), energy dispersive X-ray (EDX) and UV-Vis diffuse reflectance spectra (DRS) techniques. In the prepared nanoparticles, Cu^{2+} ions are incorporated into the ZnS lattice. The nanoparticles have absorption edges at visible light region. The SEM images demonstrate that size of the nanoparticles decreases with Cu^{2+} content. To achieve maximum degradation efficiency, the influence of various operational parameters such as mole fraction of Cu^{2+} ions, ultrasonic irradiation time, catalyst weight, calcination temperature, concentration of methylene blue (MB) and pH of solution on the degradation rate constant was investigated under visible light irradiation and the results were discussed. It was found that the degradation reaction follows pseudo first-order kinetics. The nanoparticles with 0.015 mole fraction of Cu^{2+} ions exhibit highest activity among the prepared samples.

Keywords: Cu-doped ZnS, Photocatalysis, Ultrasonic irradiation, Nanoparticles

INTRODUCTION

Many industries are widely using dyes and pigments for various purposes and their effluents can cause environmental pollution. Traditional techniques such as adsorption and coagulation by chemical agents are non-destructive and simply transfer the contaminant from water to another phase [1-3]. Then, a low-cost complete mineralization process for the dyes would find extensive use for the treatment of large volume of wastewater generated from the industries. Heterogeneous photocatalysis, an advanced oxidation technology employing semiconductors as photocatalyst, is a promising method for the treatment of contaminated water containing various organic pollutants [4-7]. This method is generally based on the generation of reactive species such as OH radicals which interact with organic pollutants leading to progressive degradation and subsequently complete mineralization [8,9]. This method is clean, low temperature and non-energy intensive approach for treatment of the pollutants. Although many photocatalysts have been developed, most of them are not highly efficient under visible light irradiation [10,11]. However, for higher photocatalytic efficiency and many practical applications, it is desirable that photocatalysts should absorb visible light due to the fact that visible light accounts for 45% of energy in the solar radiation while UV light less than 10% [12-14]. Therefore, there is a need to look for photocatalysts that absorb in the visible range and possess good activity as well [15-17].

Cu-doped ZnS is an active photocatalyst for hydrogen generation by water splitting under visible light irradiation. Kudo and Sekizawa have prepared $Zn_{0.97}Cu_{0.03}S$ solid solution and applied it for hydrogen generation in aqueous solution of Na_2SO_3 by water splitting under visible light irradiation [18,19]. Moreover, Arai and *et al.* have synthesized Cu-doped ZnS with high activity for hydrogen generation from alkaline sulfide solution [20]. Wang [21], Yang [22], Peng [23], Sambasivam [24] and their coworkers have investigated optical properties of Cu-doped ZnS nanoparticles. Recently, Mohamed has prepared thin films of Cu-dopped ZnS by electron beam evaporation on glass substrates at 1000 ºC for 2 h and investigated photocatalytic

*Corresponding author. E-mail: ahabibi@uma.ac.ir

activity of the prepared nanoparticles [25]. In addition, Pouretedal and *et al.* have prepared nanoparticles of ZnS doped with manganese, nickel and cupper in presence of mercaptoethanol as capping agent and investigated photocatalytic activities [26]. As can be seen, little work has been reported on photocatalytic degradation of organic contaminants by Cu-doped ZnS nanoparticles. Moreover, the reported preparation methods mainly have high temperature or long reaction time and most of them involved environmentally malignant chemicals and organic solvents, which are toxic and not easily degraded in the environment. Therefore, searching new methodology to prepare these nanomaterials is of great importance for both fundamental study and practical applications. Very recently, we have prepared Cu-doped ZnS by microwave irradiation and refluxing methods in water and their photocatalytic activities were investigated [27,28].

The utilization of ultrasonic irradiation (USI) for preparation of nanomaterials has been a research topic of great interest. This is due to simplicity of sonochemical method, the cheap price of the equipment and that in many cases the as-prepared material is obtained in the crystalline phase. Ultrasound induces chemical changes due to cavitation phenomena involving the formation, growth, and instantaneously implosive collapse of bubbles in liquid, which can generate local hot spots having a temperature of roughly 5000 °C, pressures of about 500 atm, and a lifetime of a few microseconds [29,30]. These extreme conditions can drive chemical reactions which have been developed to fabricate a variety of nanomaterials [31-35].

In the present paper, ultrasonic-assisted method was applied for preparation of Cu-doped ZnS nanoparticles in water as a green and template-free method. Moreover, influence of various operational parameters such as mole fraction of Cu^{2+} ions, ultrasonic irradiation time, catalyst weight, calcination temperature, concentration of methylene blue (MB) and pH of solution on photodegradation reaction of MB has been studied to achieve maximum degradation efficiency and the results were discussed.

MATERIALS AND METHODS

Materials

Zinc acetate (Zn $(CH_3COO)_2 .2H_2O$ extra pure), cupper acetate (Cu $(CH_3COO)_2 .H_2O$ extra pure), thioacetamide (TAA, CH_3CSNH_2 GR for analysis) and absolute ethanol were obtained from Merck, and employed without further purification. Double distilled water was used for the experiments.

Instruments

The ultrasound radiation was performed using dr. heilscher high intensity ultrasound processor UP200H Germany (0.7 cm diameter Ti horn, 140 W, 23 kHz). The X-ray diffraction (XRD) patterns were recorded on Ital Structures MPD3000 with Cu Kα radiation (λ = 0.15406 nm), employing scanning rate of 0.04˚/sec in the 2θ range from 20˚ to 70˚. Diffuse reflectance spectra (DRS) were recorded by a Scinco 4100 apparatus. Surface morphology and distribution of particles were studied *via* LEO 1430VP scanning electron microscopy (SEM), using an accelerating voltage of 15 kV. The purity and elemental analysis of the products were examined by energy dispersive analysis of X-rays (EDX) on the same SEM instrument. The samples used for SEM and EDX experiments were prepared by transferring the particles, which at first were dispersed in the ethanol to glass substrate attached to the SEM stage. After allowing the evaporation of ethanol from the substrate, the particles on the stage were coated with a thin layer of gold and palladium.

Preparation of the Nanoparticles

In a typical procedure for preparation of $Zn_{0.985}Cu_{0.015}S$ nanoparticles, zinc acetate dihydrate (4.258 g) and cupper acetate (0.0599 g) were dissolved in 50 ml of distilled water under stirring at room temperature. Also, 1.50 g of TAA was dissolved in 50 ml of distilled water. Then, the TAA solution was slowly added into the above mentioned solution under magnetic stirring. The titanium tip of the horn was immersed directly in the reaction solution. The solution imposed to ultrasonic irradiation for 30 min in a beaker. The formed suspension was centrifuged to get the precipitate out and washed three times with double distilled water to remove the unreacted reagents and dried in an oven at 60 °C for 48 h. In order to investigate the effect of ultrasonic irradiation time on photocatalytic activity of the nanoparticles, three more comparative samples were prepared, keeping the reaction parameters constant except

that the products were prepared by ultrasonic irradiations for 15, 60 and 120 min.

Photocatalysis Experiments

To investigate photocatalytic activity of the prepared nanoparticles, photodegradation of MB has been studied. Photocatalysis experiments were performed in a cylindrical Pyrex reactor with about 400 ml capacity. The reactor was provided with water circulation arrangement to maintain the temperature at 25 °C. The solution was magnetically stirred and continuously aerated by a pump to provide oxygen and complete mixing of the reaction solution. A tungsten lamp with 500 W was used as visible light source. The lamp was fitted on the top of the reactor. Prior to illumination, a suspension containing 0.1 g of the nanoparticles and 250 ml of MB (2.5×10^{-5} M) was continuously stirred in the dark for 30 min, to attain adsorption equilibrium. Samples were taken from the reactor at regular intervals and centrifuged to remove the photocatalyst before analysis by spectrophotometer at 664 nm corresponding to maximum absorption wavelength (λ_{max}) of MB. The adsorption capacity, q_e (mol g^{-1}), of the prepared nanoparticles was calculated by a mass-balance relationship, which represents the amount of adsorbed MB per amount of the photocatalyst [36]:

$$q_e = \frac{(C_o - C_e)V}{W} \quad (1)$$

where C_0 and C_e are concentrations of MB in solution (mol dm^{-3}) at $t = 0$ and time of equilibrium. V is the volume of the solution (dm^3), and W is weight of the photocatalyst (g). The adsorption experiments were carried out in the dark to prevent photocatalytic degradation of MB.

RESULTS AND DISCUSSION

In Fig. 1, the XRD patterns for the ZnS, $Zn_{0.985}Cu_{0.015}S$,

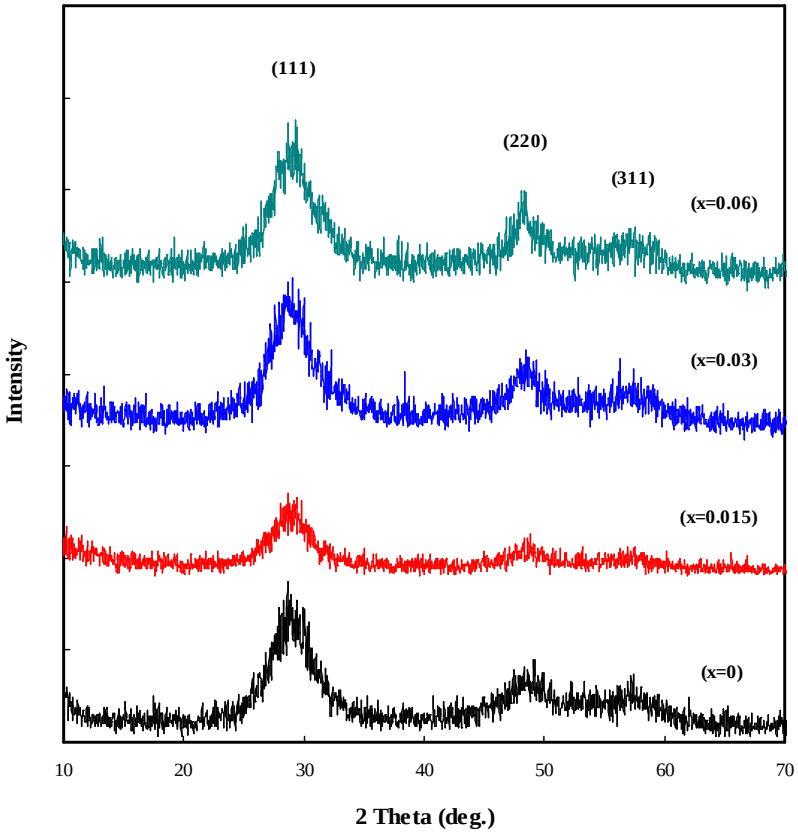

Fig. 1. Powder XRD patterns for: (a) ZnS, (b) $Zn_{0.985}Cu_{0.015}S$, (c) $Zn_{0.97}Cu_{0.03}S$ and (d) $Zn_{0.94}Cu_{0.06}$ nanoparticles.

$Zn_{0.97}Cu_{0.03}S$ and $Zn_{0.94}Cu_{0.06}S$ nanoparticles are shown. For ZnS nanoparticles, the diffraction peaks correspond to (111), (220) and (311) planes of cubic crystal system (JCPDS reference code: 5-0566). The $Zn_{0.985}Cu_{0.015}S$, $Zn_{0.97}Cu_{0.03}S$ and $Zn_{0.94}Cu_{0.06}S$ nanoparticles have the XRD patterns similar to that of the ZnS. Therefore, the prepared nanoparticles have the same crystal structure. Zinc and cupper cations have similar ionic radii (0.74 and 0.72 Å, respectively), then Cu^{2+} ions can incorporate in the ZnS lattice [37]. The XRD data are used to estimate average size of the crystallites (D) by Scherrer's equation [38]:

$$D = K\lambda\ (B\cos\theta\ ) \qquad (2)$$

where λ is the wavelength of X-ray radiation (0.15406 nm), K the Scherrer's constant (K = 0.9), θ the characteristic X-ray radiation (2θ = 29.5°) and B is the full-width-at-half-maximum of the (111) plane (in radians). The average crystallite sizes for as-prepared ZnS, $Zn_{0.985}Cu_{0.015}S$, $Zn_{0.97}Cu_{0.03}S$ and $Zn_{0.94}Cu_{0.06}S$ nanoparticles are about 2.5, 3.3, 3.3 and 2.3 nm, respectively.

Purity and composition of the prepared samples were studied by EDX technique and the results for the ZnS and $Zn_{0.985}Cu_{0.015}S$ nanoparticles are shown in Fig. 2. For the ZnS nanoparticles, the peaks are clearly related to Zn and S elements. It is clear that for the $Zn_{0.985}Cu_{0.015}S$ nanoparticles, the peaks are related to Zn, Cu and S elements. Other peaks in this figure are corresponding to the Au element applied for sputter coating of the sample.

The SEM technique was applied to study surface morphology of the nanoparticles which their records are shown in Fig. 3. It is evident that morphology of the nanoparticles is nearly spherical with various sizes. Although the particles are agglomerating, the boundaries between crystallites are observable. Moreover, size of the nanoparticles decreases with cupper content in the prepared samples.

The DRS of the nanoparticles with different cupper contents were obtained and the results are shown in Fig. 4. As can be seen, the ZnS nanoparticles do not have any absorption in the visible region. The band gap of the ZnS nanoparticles (3.85 eV) is increased compared to that of bulk ZnS (3.60 eV). The enlargement of band gap (0.25 eV) or blue shift can be attributed to the quantum confinement

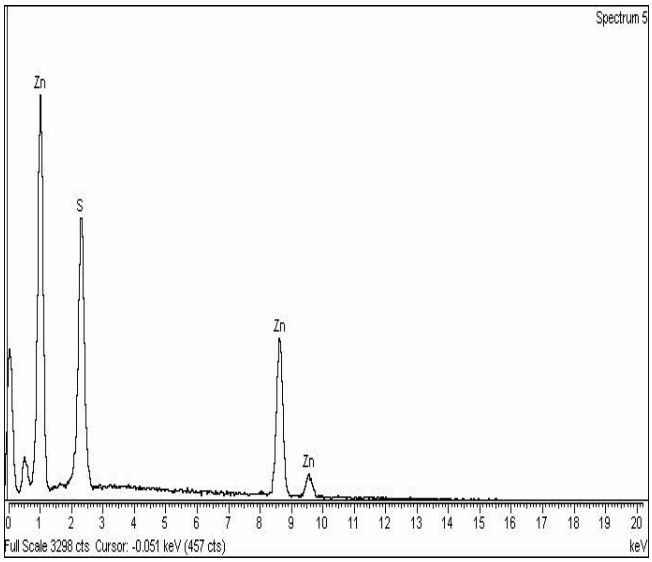

(a)

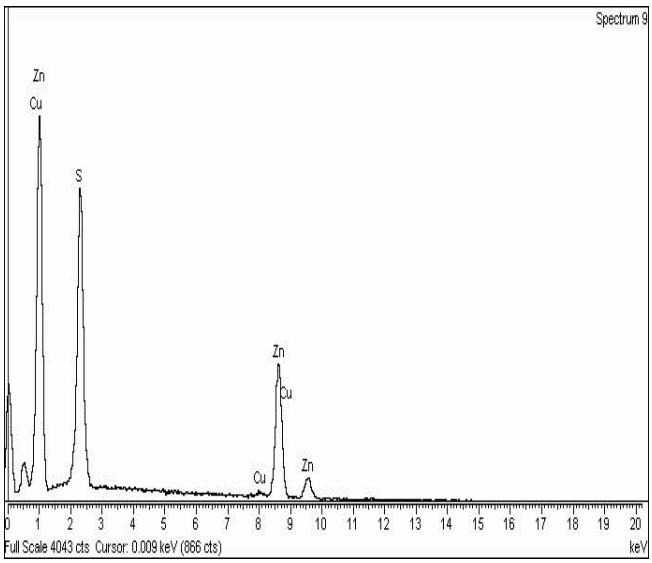

(b)

Fig. 2. The EDX results for: (a) ZnS and (b) $Zn_{0.985}Cu_{0.015}S$ nanoparticles.

effect of the ZnS nanoparticles. The nanoparticles of Cu-doped ZnS have absorption band covering visible light region. The visible light absorption for the nanoparticles increases by increasing Cu^{2+} ion content.

The results demonstrate that the nanoparticles have ability for adsorption of MB molecules. To prevent

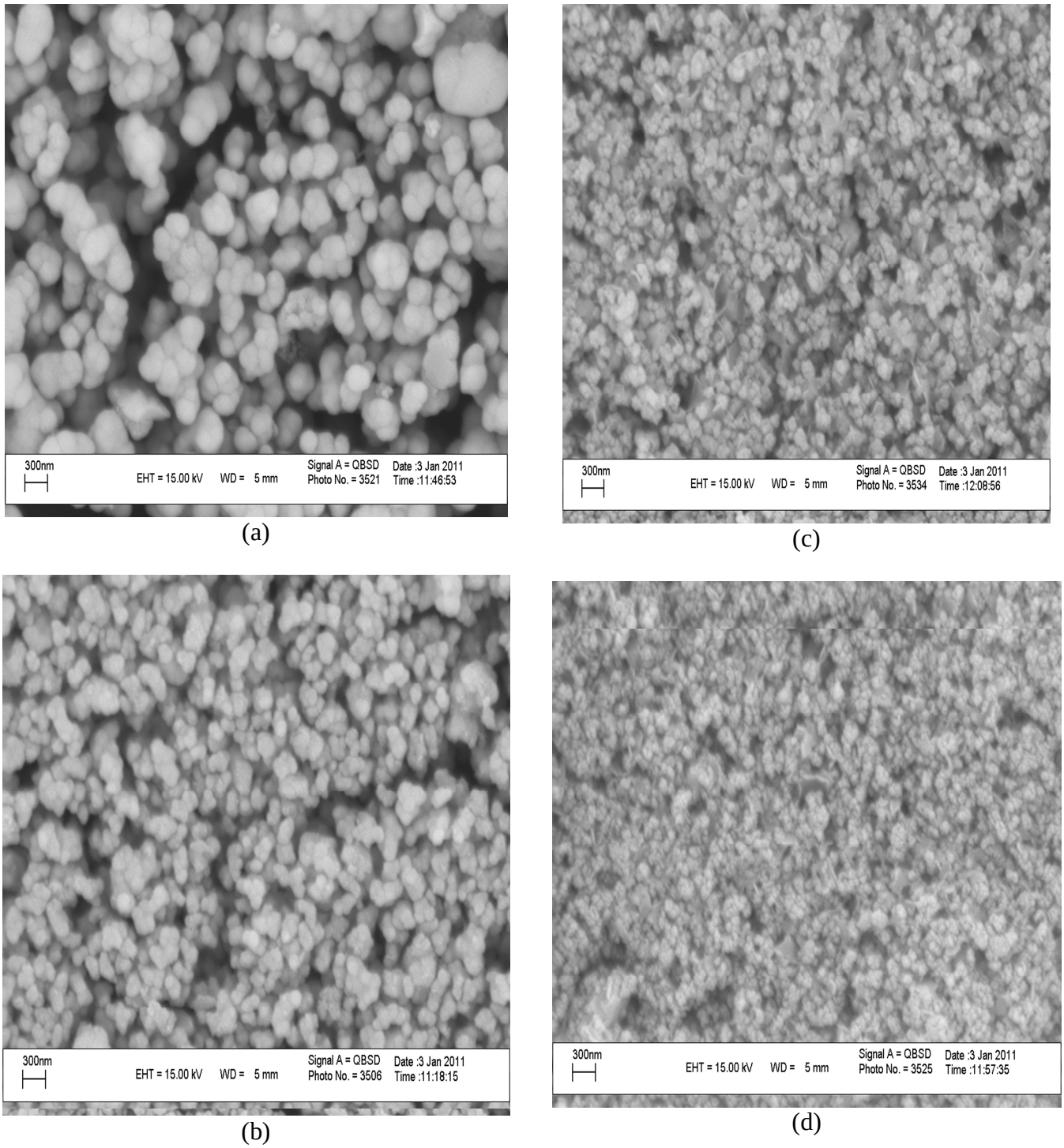

Fig. 3. SEM images for: (a) ZnS, (b) $Zn_{0.985}Cu_{0.015}S$, (c) $Zn_{0.97}Cu_{0.03}S$ and (d) $Zn_{0.94}Cu_{0.06}$ nanoparticles.

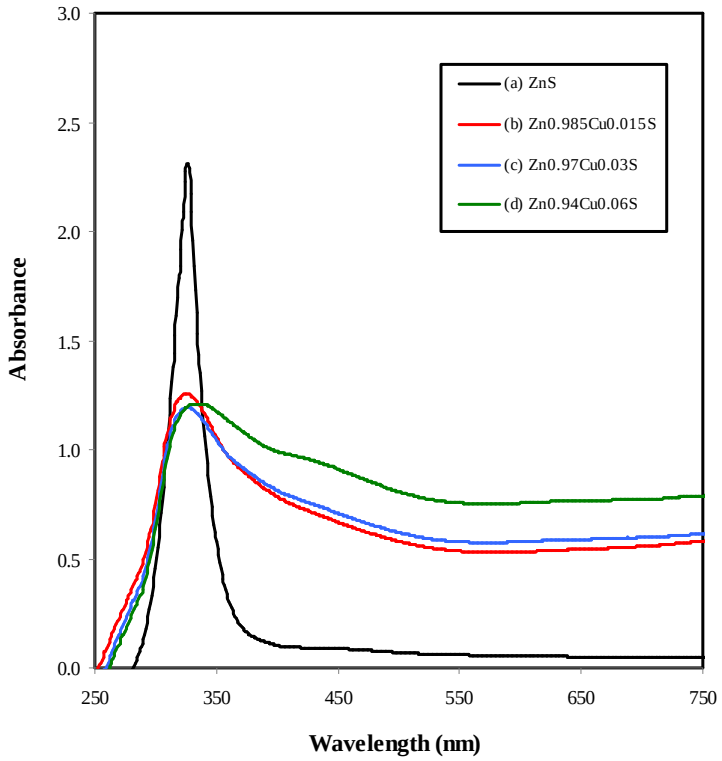

Fig. 4. Diffuse reflectance spectra for: (a) ZnS, (b) $Zn_{0.985}Cu_{0.015}S$, (c) $Zn_{0.97}Cu_{0.03}S$ and (d) $Zn_{0.94}Cu_{0.06}$ nanoparticles.

photocatalytic degradation of the dye, the adsorption experiments were carried out in dark. Plot of absorbance at 664 nm for adsorption of MB on the nanoparticles *versus* time are demonstrated in Fig. 5. The adsorption capacity (q_e) of the prepared samples was calculated using Eq. (1) after 550 min and the results were tabulated (Table 1). It is clear that the ZnS nanoparticles have very lower ability for adsorption of MB molecules. Moreover, adsorption capacity of the nanoparticles increases with cupper content. The SEM images demonstrated that size of the nanoparticles decreases with cupper content. Then, increase of the adsorption capacity of the nanoparticles can be attributed to increasing the surface area with decreasing particle size [39]. Among the prepared Cu-doped nanoparticles, $Zn_{0.985}Cu_{0.015}S$ nanoparticles have very lower tendency for adsorption of MB molecules.

Photocatalytic activity of the prepared samples was investigated by degradation of MB. In Fig. 6, photodegradation of the dye on the nanoparticles are shown. As can be seen, all of the Cu-doped ZnS nanoparticles exhibit higher activity than that of the pure ZnS.

Increasing the photocatalytic activity of the Cu-doped ZnS nanoparticles relative to the ZnS nanoparticles can be attributed to increasing visible light absorption by the photocatalyst due to the presence of Cu^{2+} ions [40,41]. In addition, trapping of charge carriers is one of the methods to decrease electron-hole recombination rate and extend life time of the charge carriers. It has been reported that some transition metal dopants can act as the trapping sites to decrease the electron-hole recombination rate [42,43]. Then, presence of Cu^{2+} ions in the nanoparticles enhances the photocatalytic activity with increasing visible light absorption and electron-hole life time.

To obtain maximum degradation efficiency of MB on $Zn_{0.985}Cu_{0.015}S$ nanoparticles with lower adsorption capacity and higher photocatalytic activity, the reaction variables were optimized. The essential reaction parameters of (i) ultrasonic irradiation time, (ii) catalyst weight, (iii) calcination temperature, (iv) initial MB concentration and (v) pH of solution were varied which the results are

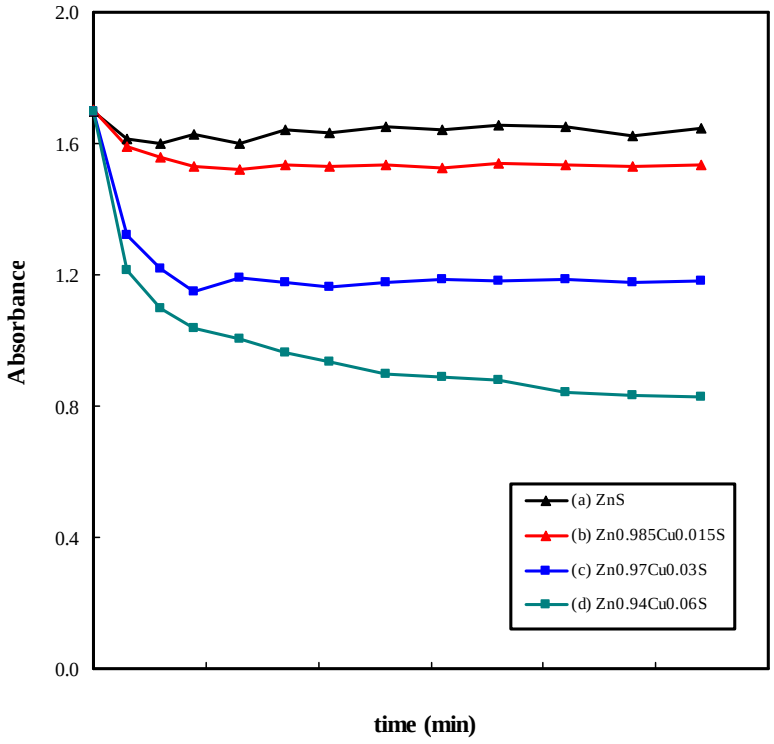

Fig. 5. Adsorption of MB on: (a) ZnS, (b) $Zn_{0.985}Cu_{0.015}S$, (c) $Zn_{0.97}Cu_{0.03}S$ and (d) $Zn_{0.94}Cu_{0.06}$ nanoparticles.

Table 1. Adsorption Capacity Along with Adsorption Percent of Methylene Blue Molecules on $Zn_{1-x}Cu_xS$ Nanoparticles at 25 ºC

No.	Nanoparticle	q_e (mol g^{-1})	Adsorption percent
1	ZnS	2.01×10^{-6}	3.06
2	$Zn_{0.985}Cu_{0.015}S$	6.32×10^{-6}	9.82
3	$Zn_{0.97}Cu_{0.03}S$	1.96×10^{-5}	30.5
4	$Zn_{0.94}Cu_{0.06}S$	3.30×10^{-5}	51.2

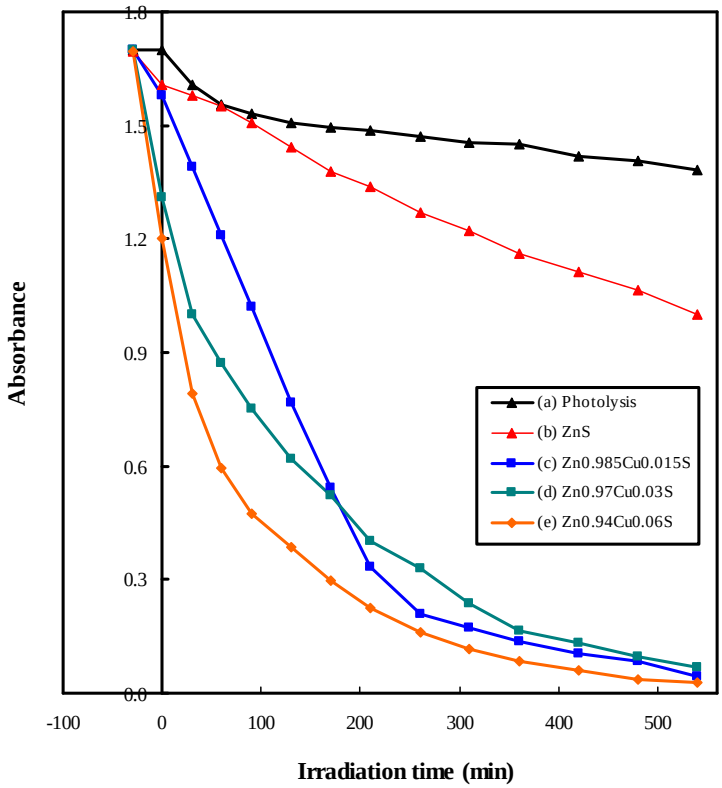

Fig. 6. Photodegradation of MB on: (a) ZnS, (b) $Zn_{0.985}Cu_{0.015}S$, (c) $Zn_{0.97}Cu_{0.03}S$ and (d) $Zn_{0.94}Cu_{0.06}$ nanoparticles.

discussed in the following sections.

Effect of Ultrasonic Irradiation Time

To examine the influence of ultrasonic irradiation time applied for preparation of the $Zn_{0.985}Cu_{0.015}S$ nanoparticles on the photocatalytic activity, three more comparative samples were prepared, keeping the reaction parameters constant except that the nanoparticles were prepared by irradiation for 15, 60 and 120 minutes. Degradation of MB under visible light irradiation on the nanoparticles prepared at various ultrasonic irradiation times is demonstrated in Fig. 7. As can be seen, ultrasonic irradiation time has not remarkable effect on the degradation reaction.

Effect of the Catalyst Weight

Generally, photocatalytic activity of semiconductors depends on photocatalyst weight [44]. Hence a series of experiments were carried out to find the optimum catalyst amount by varying weight of the $Zn_{0.985}Cu_{0.015}S$ nanoparticles between 0.01 and 0.15 g.

Dependence of photocatalytic reaction rate on concentration of organic pollutants is well described by the following kinetic model [45]:

$$rate = -\frac{d[MB]}{dt} = \frac{kK[MB]}{1+K[MB]} \quad (3)$$

where k is the first-order rate constant of the reaction and K is adsorption constant of MB on the photocatalyst. Equation (3) can be simplified to a pseudo first-order equation [45]:

$$\ln\frac{[MB]_o}{[MB]} = kKt = k_{obs}t \quad (4)$$

in which k_{obs} is the observed first-order rate constant of the degradation reaction. In order to examine whether the reaction rate could be congruent with a pseudo first-order reaction under different conditions, plots of ln*[MB]* or ln*A* (absorbance) *vs.* irradiation time, were considered for the

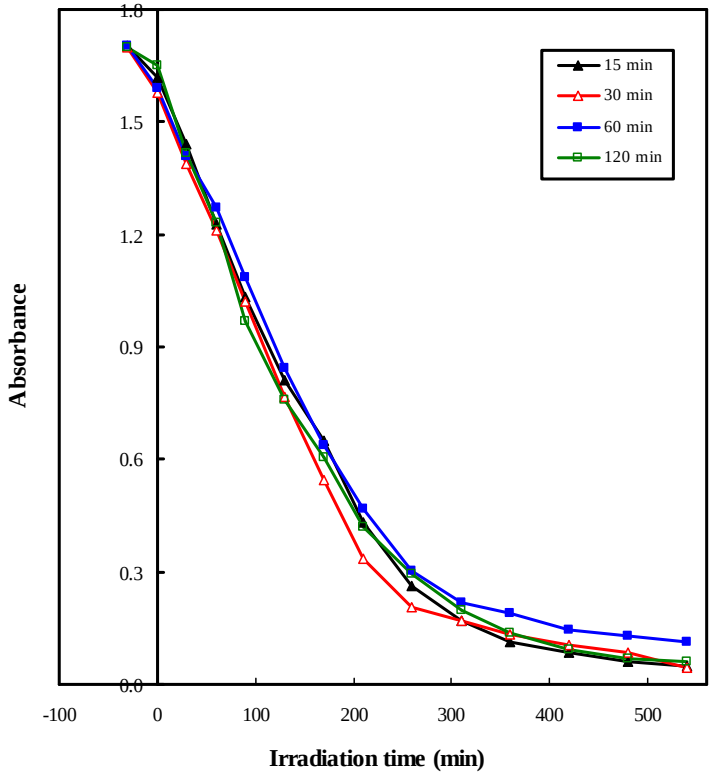

Fig. 7. Plot of absorbance *vs.* irradiation time for degradation of MB on $Zn_{0.985}Cu_{0.015}S$ nanoparticles prepared by different ultrasonic irradiation times.

prepared nanoparticles. For example, Fig. 8 demonstrates plot of ln*A* *vs.* irradiation time for MB degradation on the $Zn_{0.985}Cu_{0.015}S$ nanoparticles. As can be seen, well linear correlation existed between ln*A* and irradiation time. In Fig. 9, the rate constant of the reaction has been plotted *vs.* weight of the photocatalyst. As can be seen, the degradation rate constant increases with increasing weight of the photocatalyst and then decreases. Indeed, maximum value was achieved at 0.05 g of the photocatalyst. In general, with increasing weight of the photocatalyst, the reaction rates should be increased, due to the fact that active sites of the photocatalyst are increased [44]. However, more photocatalyst would also induce greater aggregation of the photocatalyst and the specific surface area decreased, leading to a reduction in the reaction rate. Moreover, this can be attributed to the scattering of light and reduction in light penetration through the solution [46].

Effect of Calcination Temperature

Photocatalytic activity generally depends on calcination temperature. In order to investigate the effect of calcination temperature, degradation of MB on the $Zn_{0.985}Cu_{0.015}S$ nanoparticles calcined at various temperatures was considered (Fig. 10). The degradation rate constant on the nanoparticles without calcination and the catalysts calcined at 200, 300 and 400 ºC are 8.44×10^{-3}, 6.48×10^{-3}, 5.49×10^{-3} and 2.33×10^{-3} min^{-1}, respectively. Then, the rate constant decreases with calcination temperature. Decreasing the rate constant for photocatalytic degradation of MB is attributed to aggregation of the photocatalyst [47].

Effect of MB Concentration

The effect of MB concentration on the degradation rate constant was investigated by varying the initial concentration between 7.0×10^{-6} and 3.0×10^{-5} M with

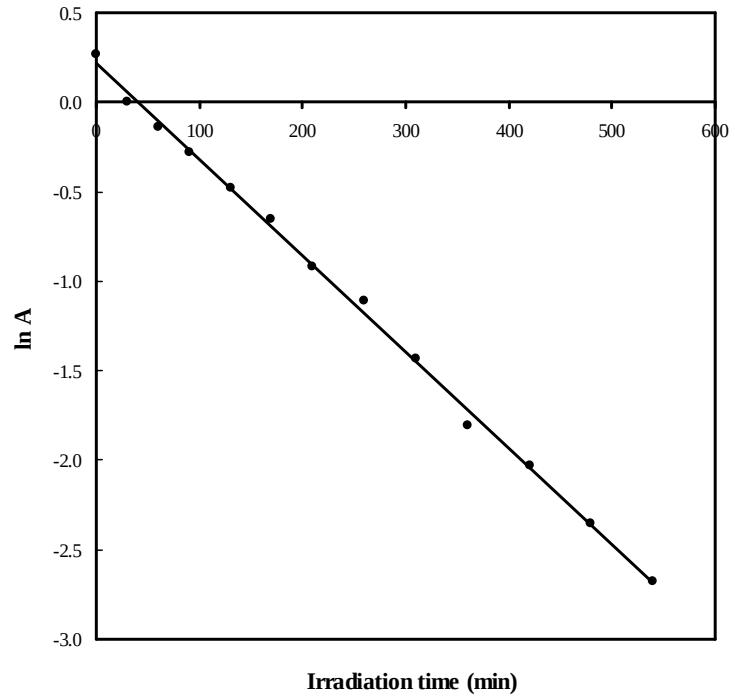

Fig. 8. Plot of ln*A vs.* irradiation time for degradation of MB on $Zn_{0.985}Cu_{0.015}S$ nanoparticles.

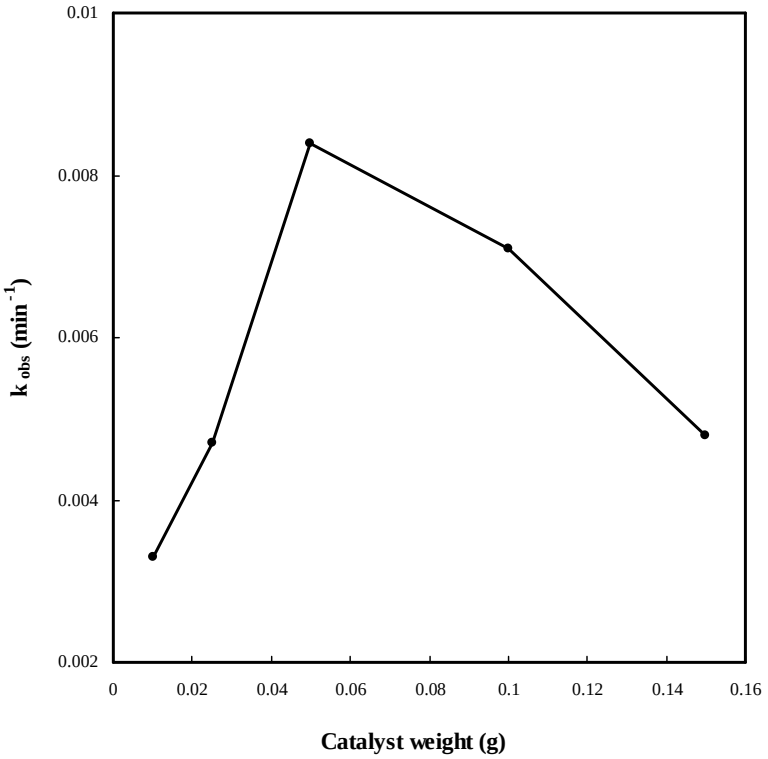

Fig. 9. Plot of observed first-order rate constant of the degradation reaction *vs.* the photocatalyst weight.

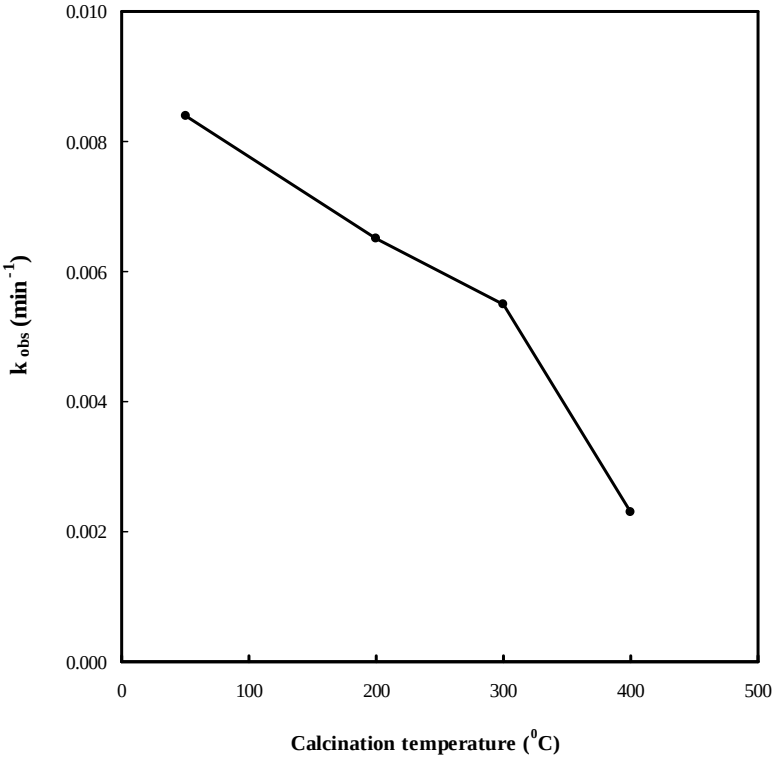

Fig. 10. Plot of observed first-order rate constant of the degradation reaction *vs.* calcination temperature.

constant catalyst weight of 0.05 g (Fig. 11). As can be seen, the rate constant decreases with increasing the concentration of MB. When the initial concentration increases, more organic substances are adsorbed on the surface of the photocatalyst. Therefore, there will be lower active sites for generation of reactive species. The formation of reactive species has main role in degradation reactions [48], then the rate constant decreases with concentration of MB. Moreover, with increasing concentration of MB, the photons get intercepted before they can reach the catalyst surface and screening effect dominated, preventing penetration of the light on the photocatalyst, consequently the degradation rate is reduced [49].

Effect of Solution pH

The pH of solution is an important variable in aqueous phase mediated photocatalytic reactions [50]. The effect of pH on the rate constant was studied by keeping all other experimental conditions constant and varying the initial pH from 3 to 11 (Fig. 12). As can be seen, the rate constant suddenly increases with increasing in pH and then decreases. Increase of the rate constant with increasing pH of solution is due to increase in adsorption of MB on surface of the catalyst. The zero point charge pH for the catalyst will be about at neutral solution [26]. At low pH, the photocatalyst surface is positively charged and repulsive forces between the photocatalyst and the cationic dye will lead to a decrease in MB adsorption and the degradation rate constant. Furthermore, the nanoparticles have tendency to dissolve with decreasing pH of solution [51]:

$$Zn_{0.985}Cu_{0.015}S + 2H^+ \longrightarrow 0.985Zn^{2+} + 0.015Cu^{2+} + H_2S \quad (5)$$

Therefore, in acidic solutions the photocatalyst have low stability and the rate constant is decreased suddenly with decreasing pH of solution. Above zero point charge pH, surface of the photocatalyst is negatively charged by means of adsorbed OH^-. Therefore, electrostatic attraction between surface of the photocatalyst with negative charge and the

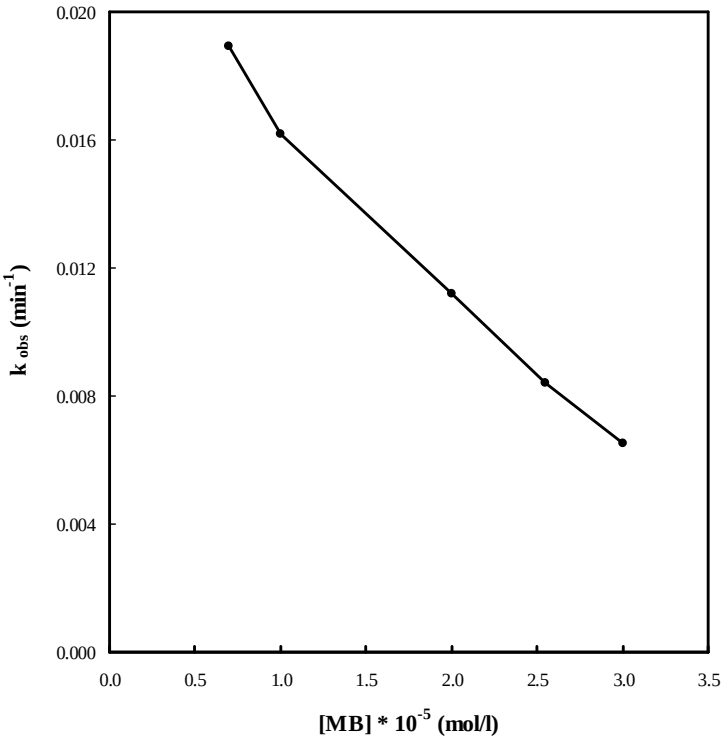

Fig. 11. Plot of observed first-order rate constant of the degradation reaction *versus* concentration of MB.

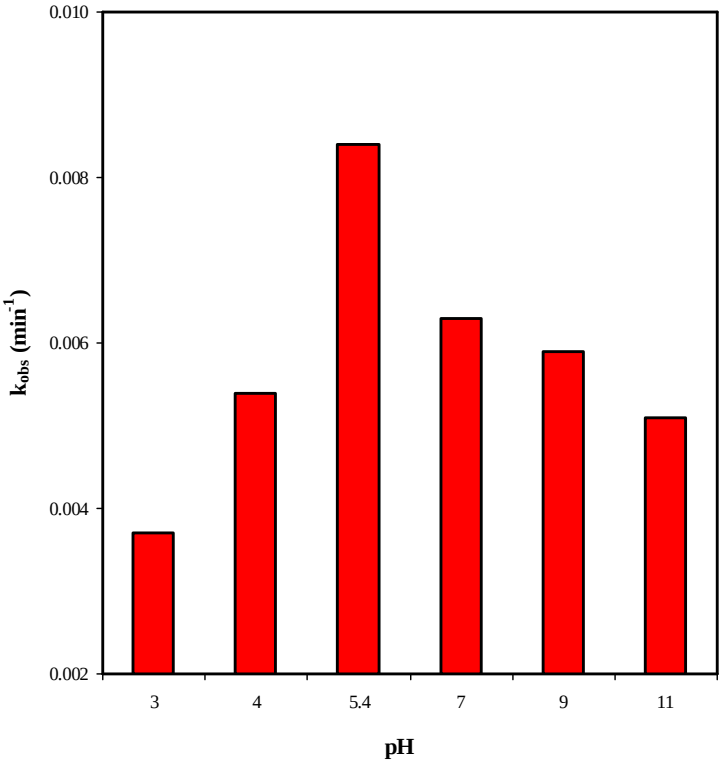

Fig. 12. Effect of pH of solution on degradation rate constant of MB on $Zn_{0.985}Cu_{0.015}S$ nanoparticles.

cationic dye favors adsorption of MB. For this reason, the solution with pH 5.4 is proper for the degradation reaction.

Mechanism of the Degradation Reaction

After illumination of Cu-doped ZnS nanoparticles by visible light irradiation, electron-hole pairs are produced as the beginning of the reactions [52]. After that, reactive species are formed by the following processes. In presence of the reactive species, MB molecules are degraded to produce the degradation products [52,53].

$$\text{Cu-doped ZnS} + h\nu\ (\text{visible}) \longrightarrow \text{Cu-doped ZnS } (e^-_{CB} + h^+_{VB}) \quad (6)$$

$$\text{Cu-doped ZnS } (e^-_{CB} + h^+_{VB}) \longrightarrow \text{Cu-doped ZnS} + \text{heat} \quad (7)$$

$$e^-_{CB}\ (\text{Cu-doped ZnS}) + O_2 \longrightarrow {}^{\bullet}O_2^- \quad (8)$$

$${}^{\bullet}O_2^- + H^+ \longrightarrow {}^{\bullet}OOH \quad (9)$$

$${}^{\bullet}OOH + e^-_{CB}\ (\text{Cu-doped ZnO}) + H^+ \longrightarrow H_2O_2 \longrightarrow 2\,{}^{\bullet}OH \quad (10)$$

$$MB + {}^{\bullet}OH/h^+/{}^{\bullet}O_2^- \longrightarrow \text{intermediates} \longrightarrow \text{degradation products} \quad (11)$$

CONCLUSIONS

A template-free and green method was applied for preparation of Cu-doped ZnS nanoparticles in water. The nanoparticles were characterized by different techniques. Photocatalytic activity of the nanoparticles towards degradation of MB was evaluated under visible light irradiation. The photocatalytic activity of the Cu-doped ZnS nanoparticles is higher than that of the pure ZnS. To achieve maximum degradation efficiency, the influence of various operational parameters such as ultrasonic irradiation time, catalyst weight, calcination temperature, concentration of MB and pH of solution on the degradation reaction was studied and the results were discussed. The results demonstrate that the rate constant decreases with concentration of MB and calcination temperature. Moreover, there are maxima in correlation of the reaction rate with catalyst weight and pH of solution.

ACKNOWLEDGMENTS

The Authors wish to acknowledge University of Mohaghegh Ardabili, for financial support of this work.

REFERENCES

[1] O. Ozdemir, B. Armagan, M. Turan, M.S. Celik, Dyes Pigments 62 (2004) 49.
[2] S. Wang, H. Li, S. Xie, S. Liu, L. Xu, Chemosphere 65 (2006) 82.
[3] P.P. Selvam, S. Preethi, P. Basakaralingam, N. Thinakaran, A. Sivasamy, S. Sivanesan, J. Hazard. Mater. 155 (2008) 39.
[4] P.R. Gogate, A.B. Pandit, Adv. Environ. Res. 8 (2004) 501.
[5] K. Kabra, R. Chaudhary, R.L. Sawhney, Ind. Eng. Chem. Res. 43 (2004) 7683.
[6] M.P. Reddy, A. Venugopal, M. Subrahmanyam, Appl. Catal. B: Environ. 69 (2006) 164.
[7] N. Sobana, M. Muruganandam, M. Swaminathan, Catal. Commun. 9 (2008) 262.
[8] C.-H. Wu, J.-M. Chern, Ind. Eng. Chem. Res. 45 (2006) 6450.
[9] S.J. Teichner, J. Porous Mater. 15 (2008) 311.
[10] R. Yuan, R. Guan, W. Shen, J. Zheng, J. Colloid Interface Sci. 282 (2005) 87.
[11] T. Tachikawa, M. Fujitsuka, T. Majima, J. Phys. Chem. C 111 (2007) 5259.
[12] N. Dubey, S.S. Rayalu, N.K. Labhsetwar, S. Devotta, Int. J. Hydrogen Energy 33 (2008) 5958.
[13] W. Su, J. Chen, L. Wu, X. Wang, X. Fu, Appl. Catal. B: Envir. 77 (2008) 264.
[14] J. Sun, L. Qiao, S. Sun, G. Wang, J. Hazard. Mater. 155 (2008) 312.
[15] N. Dubey, S.S. Rayalu, N.K. Labhsetwar, S. Devotta, Int. J. Hydrogen Energy 33 (2008) 5958.
[16] L.-C. Chen, Y.-J. Tu, Y.-S. Wang, R.-S. Kan, C.-M. Huang, J. Photochem. Photobiol. A: Chem. 199 (2008) 170.
[17] H. Xia, H. Zhuang, T. Zhang, D. Xiao, Mater. Lett. 62 (2008) 1126.

[18] A. Kudo, M. Sekizawa, Catal. Lett. 58 (1999) 241.
[19] A. Kudo, M. Sekizawa, Chem. Commun. (2000) 1371.
[20] T. Arai, S.-I. Senda, Y. Sato, H. Takahashi, K. Shinoda, B. Jeyadevan, K. Tohji, Chem. Mater. 20 (2008) 1997.
[21] M. Wang, L. Sun, X. Fu, C. Liao, C. Yan, Solid State Commun. 115 (2000) 493.
[22] P. Yang, C. Song, M. Lu, G. Zhou, Z. Yang, D. Xu, D. Yuan, J. Phys. Chem. Solids 63 (2002) 639.
[23] W.Q. Peng, G.W. Cong, S.C. Qu, Z.G. Wang, Optical Mater. 29 (2006) 313.
[24] S. Sambasivam, B. Sathyaseelan, D.R. Reddy, B.K. Reddy, C.K. Jayasankar, Spectrochim. Acta A: Mol. Biomolec. Spect. 71 (2008) 1503.
[25] S.H. Mohamed, J. Phys. D: Appl. Phys. 43 (2010) 35406.
[26] H.R. Pouretedal, A. Norozi, M.H. Keshavarz, A. Semnani, J. Hazard. Mater. 162 (2009) 674.
[27] S. Naghiloo, A. Habibi-Yangjeh, M. Behboudnia, Appl. Surf. Sci. 257 (2011) 2361.
[28] Z. Poormohammadi-Ahandani, A. Habibi-Yangjeh, Desalination 271 (2011) 273.
[29] K.S. Suslick, S.B. Choe, A.A. Cichowals, M.W. Grinstaff, Nature 353 (1991) 414.
[30] G.J. Price, Current Trends in Sonochemistry, Royal Society of Chemistry, Cambridge, 1992.
[31] V.G. Pol, A. Gedanken, J. Chem. Mater. 15 (2003) 1111.
[32] T. Gao, Q.H. Li, T.H. Wang, Chem. Mater. 17 (2005) 887.
[33] X. Hou, F. Zhou, Y. Sun, W. Liu, Mater. Lett. 61 (2007) 1789.
[34] C. Yu, M. Yu, C. Li, X. Liu, J. Yang, P. Yang, J. Lin, J. Solid State Chem.182 (2009) 339.
[35] M. Shang, W. Wang, L. Zhou, S. Sun, W. Yin, J. Hazard. Mater. 172 (2009) 338.
[36] F. Jafari-Zare, A. Habibi-Yangjeh, Chin. J. Chem. 28 (2010) 349.
[37] W. Zhang, Z. Zhong, Y. Wang, R. Xu, J. Phys. Chem. C 112 (2008) 17635.
[38] B.D Cullity, Elements of X-ray diffraction, 2nd ed., London: Addision Wesley, 1978.
[39] L. Wang, L. Chang, B. Zhao, Z. Yuan, G. Shao, W. Zheng, Inorg. Chem. 47 (2008) 1443.
[40] J. Tang, Z. Zou, J. Ye, Chem. Mater. 16 (2004) 1644.
[41] M. Oztas, M. Bedir, A.N. Yazici, E.V. Kafadar, H. Toktamıs, Physica B 381 (2006) 40.
[42] M.A. Fox, M.T. Dulay, Chem. Rev. 93 (1993) 341.
[43] W. Zhang, Z. Zhong, Y. Wang, R. Xu, J. Phys. Chem. C 112 (2008) 17635.
[44] S. Sakthivel, B. Neppolian, M.V. Shankar, B. Arabindoo, M. Palanichamy, V. Murugesan, Sol. Energy Mater. Sol. Cells 77 (2003) 65.
[45] M.A. Behnajady, N. Modirshahla, R. Hamzavi, J. Hazard. Mater. B 133 (2006) 226.
[46] N. Daneshvar, D. Salari, A.R. Khataee, J. Photochem. Photobiol. A: Chem. 157 (2003) 111.
[47] C.-C. Wang, C.-K. Lee, M.-D. Lyu, L.-C. Juang, Dyes Pigments 76 (2008) 817.
[48] M.V. Shankar, B. Neppolian, S. Sakthivel, M. Banumathi Arabindoo, V. Palanichamy, Murugesan: Ind. J. Eng. Mater. Sci. 8 (2001) 104.
[49] S. Chakrabarti, B.K. Dutta, J. Hazard. Mater. B 112 (2004) 269.
[50] M.V. Shankar, S. Anandan, N. Venkatachalam, B. Arabindoo, V. Murugesan, J. Chem. Technol. Biotechnol. 79 (2004) 1279.
[51] N. Daneshvar, D. Salari, A.R. Khataee, J. Photochem. Photobiol. A: Chem. 162 (2004) 317.
[52] L.S. Zhang, K.H. Wong, H.Y. Yip, C. Hu, J.C. Yu, C.Y. Chan, P.K. Wong, Environ. Sci. Technol. 44 (2010) 1392.
[53] G.T. Li, K.H. Wong, X.W. Zhang, C. Hu, J.C. Yu, R.C.Y. Chan, P.K. Wong, Chemosphere 76 (2009) 1185.